Letter | Editors' Suggestion

Weak-coupling theory of magic-angle twisted bilayer graphene

Jihang Zhu [1,2], Iacopo Torre [3], Marco Polini,[4,5,3] and A. H. MacDonald [6]

[1]*Condensed Matter Theory Center and Joint Quantum Institute, Department of Physics, University of Maryland, College Park, Maryland 20742, USA*

[2]*Max Planck Institute for the Physics of Complex Systems, 01187 Dresden, Germany*

[3]*ICFO-Institut de Ciències Fotòniques, The Barcelona Institute of Science and Technology, Av. Carl Friedrich Gauss 3, 08860 Castelldefels (Barcelona), Spain*

[4]*Dipartimento di Fisica dell'Università di Pisa, Largo Bruno Pontecorvo 3, I-56127 Pisa, Italy*

[5]*Istituto Italiano di Tecnologia, Graphene Labs, Via Morego 30, I-16163 Genova, Italy*

[6]*Department of Physics, University of Texas at Austin, Austin, Texas 78712, USA*

(Received 21 December 2023; revised 30 July 2024; accepted 6 September 2024; published 20 September 2024)

Strong correlations occur in magic-angle twisted bilayer graphene (MATBG) when the octet of flat moiré minibands centered on charge neutrality (CN) is partially occupied. The octet consists of a single valence band and a single conduction band for each of four degenerate spin-valley flavors. Motivated by the importance of Hartree electrostatic interactions in determining the filling-factor-dependent band structure, we use a time-dependent Hartree approximation to gain insight into electronic correlations. We find that the electronic compressibility is dominated by Hartree interactions, that paramagnetic states are stable over a range of density near CN, and that the dependence of energy on flavor polarization is strongly overestimated by mean-field theory.

DOI: 10.1103/PhysRevB.110.L121117

Introduction. The energy bands of twisted bilayer graphene (TBG) have a four-fold spin-valley flavor degeneracy. As a magic twist angle near $\theta = 1^\circ$ is approached, the two sets of four-fold degenerate bands closest to the neutral system Fermi energy approach each other and narrow [1], converting graphene from a weakly correlated Fermi liquid to a strongly correlated system [2–5] with a rich variety of competing states, including superconductors, insulating flavor ferromagnets, and metallic flavor ferromagnets. The ferromagnetism is reminiscent of but distinct from that exhibited by Bernal-stacked bilayer graphene in the quantum Hall regime [6–13] and is now clearly established [3,5,14–32] as a prominent part of the physics of magic-angle twisted bilayer graphene (MATBG). In contrast to the quantum Hall case, in which eight Landau bands are filled sequentially to minimize the exchange energy, MATBG ground states appear [33] not to have any broken symmetries for a range of filling factors near CN, and in broken symmetry states to keep the filling factors of partially occupied flavors ν_f inside an interval $(-\nu_h^*, \nu_e^*)$, where ν_h^* and ν_e^* are the maximum hole and electron filling factors. [$\nu_f \equiv (N_f - M)/M$ where N_f is the number of flat band electrons with flavor f and M is the number of moiré cells in the system; $\nu = \sum_f \nu_f$.]

In this Letter, we address some unusual aspects of the correlation physics of MATBG from the weak-coupling point of view (one-shot *GW* approximation). We find that the average compressibility is dominated by Hartree interactions, that unbroken symmetry states are stable over a range of density near CN, and that the dependence of energy on flavor polarization is strongly overestimated by mean-field theory. Below we first explain the technical details of our calculations and then discuss the relationship of our findings to those obtained using other approaches to MATBG interaction physics.

Moiré-Band Weak-Coupling Theory. The one-shot *GW* approximation, also known as the random phase approximation (RPA), is a perturbative method that accounts for dynamic screening of long-range Coulomb interactions. It is commonly used [34,35] in *ab initio* electronic structure theory to understand collective electronic behaviors, especially as probed by optical or photoemission spectroscopy. Although rigorously justified [36] only in weakly interacting systems, it has recently attracted interest [37] as a universal and accurate method for total energy calculations in many real materials, including [38] strongly correlated Mott insulators.

In this Letter we employ RPA theory to approximate the dependence of energy on the total band filling factor and on the partitioning of electrons between the four spin-valley flavors of MATBG. Because the number of electrons for each flavor is a good quantum number, we can approximate the magnetic energy landscape by adding exchange-correlation (xc) corrections $E_{\rm xc}$ to the self-consistent Hartree (SCH) energies of flavor polarized states. The RPA theory is motivated by the unusual property of MATBG, illustrated in Fig. 1 by plotting SCH bands at a series of band filling factors and that the band filling dependence of its total energy is dominated [39–43] by a Hartree mean-field contribution. The SCH energy increases rapidly as the flat bands are filled as shown in

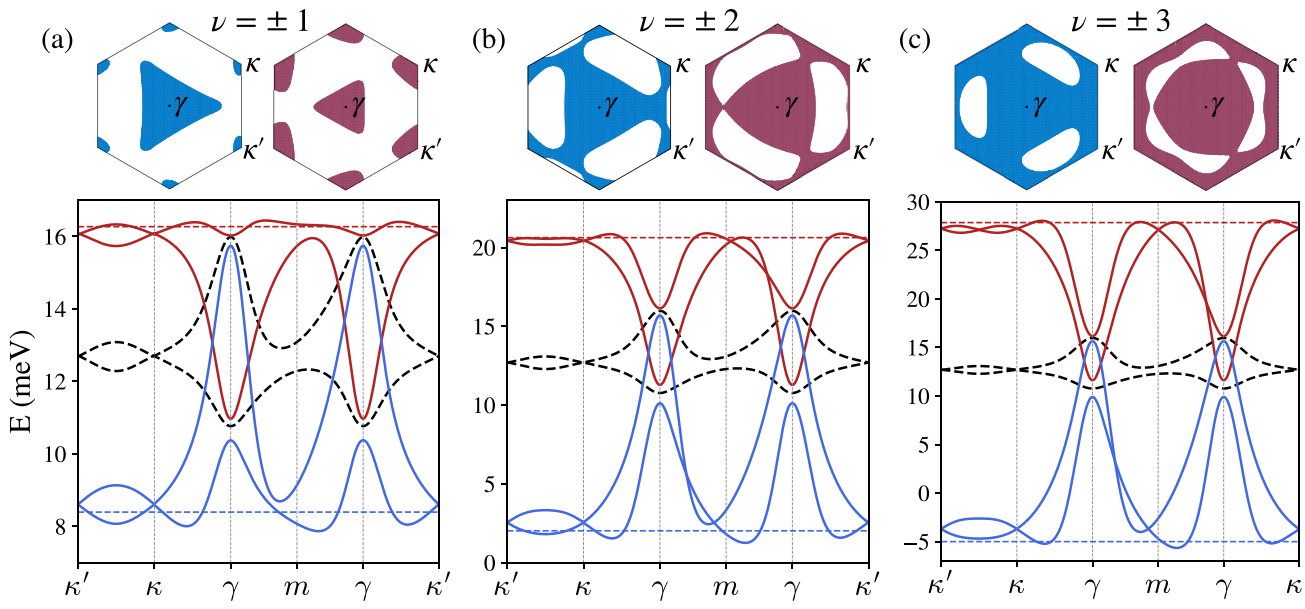

FIG. 1. The SCH paramagnetic state bands (colored lines) and corresponding Fermi surfaces (shaded areas) at a series of ν values on hole-doped (blue) and electron-doped (red) sides. The black dashed line in each spectrum is the single-particle band structure and the colored dashed horizontal lines mark Fermi levels. At $\nu = -3$, the flat valence band is 1/4 full and the occupied states are those whose charge density is most peaked near minima of the external potential produced by remote band charges. At $\nu = -1$, the flat valence band is at 3/4 filling. Holes in the valence band remain near γ, which would be the valence band bottom if Hartree corrections were not included. Holes near γ are finally filled only around $\nu = -0.3$ (see Fig. S2) as ν approaches zero and Hartree energies finally become small compared to band energies. The Fermi surfaces at filling factors $+\nu$ and $-\nu$ (for example $\nu = 2$ and $\nu = -2$) would be identical for any ν if the model had exact particle-hole symmetry. At filling factors away from $\nu = 0$, the SCH band width is dominated by the Hartree mean-field contribution.

Fig. 2(c), and dominates the experimentally measured compressibility. The RPA accounts both for this energy and for dynamic fluctuation corrections to it.

The xc correction to the SCH energy can be expressed [44] in terms of a coupling-constant integral of the pair correlation function. This quantity can, in turn, be related to the density response function by

$$E_{\rm xc} = \frac{1}{2}\sum_{\mathbf{q},\mathbf{g}}{}' V_{\mathbf{q}+\mathbf{g}}\Big[-\frac{1}{\pi}\int_0^1 d\lambda \int_0^\infty d\omega\, \chi^{\mathbf{gg}}(\mathbf{q}, i\omega; \lambda) - 1\Big], \tag{1}$$

where $V_{\mathbf{q}} = 2\pi e^2/q\epsilon_{\rm BN}$ is the two-dimensional (2D) Coulomb interaction accounting for hexagonal boron nitride (hBN) dielectric screening with the dielectric constant chosen to be $\epsilon_{\rm BN} = 5.1$ throughout the Letter, $\mathbf{q}$ is a wave vector in the moiré Brillouin zone (MBZ), $\mathbf{g}$ is a moiré reciprocal lattice vector, and the prime on the sum excludes the $\mathbf{q} = \mathbf{g} = \mathbf{0}$ term which contributes only a gate-geometry-dependent constant [44]. In Eq. (1) $\chi^{\mathbf{gg}}$ is a diagonal matrix element of the density response function, which is a matrix in reciprocal lattice vectors because of the system's discrete translational symmetry and the frequency integration used

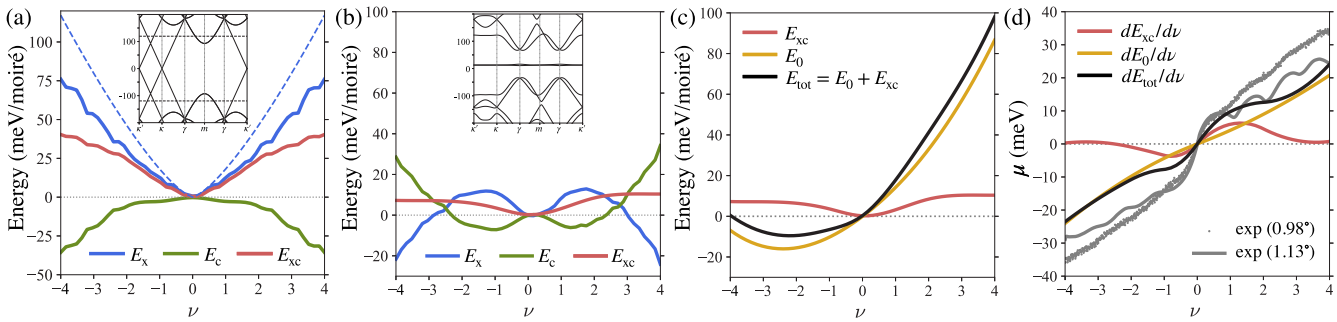

FIG. 2. Energies of paramagnetic states as a function of $\nu \in [-4, 4]$ for (a) a decoupled-bilayer and (b)–(d) 1.1°-TBG. (a,b) Exchange ($E_{\rm x}$) and RPA correlation ($E_{\rm c}$) energies as defined in Eqs. (4) and (5). The insets show the corresponding single-particle band structures. The black dashed lines in the inset of (a) mark the Fermi level for $\nu = \pm 4$. The blue dashed line in (a) is the exchange energy calculated using the approximate analytical expression Eq. (6). (c) The SCH energy E_0 [44] and the RPA total energy $E_{\rm tot}$. (d) The calculated chemical potential $\mu = dE_{\rm tot}/d\nu$ with its zero shifted to the chemical potential at $\nu = 0$. The grey dots (0.98°) and the grey line (1.13°) plot measured chemical potentials from Ref. [19]. All energies are given relative to CN with the zero of energy at the neutral system Fermi level.

to obtain equal time correlations has been rotated to the imaginary axis.

Equation (1) is formally exact. In RPA (time-dependent Hartree approximation) we replace χ in Eq. (1) by

$$\chi(\lambda) = \tilde{\chi}_{\rm H}(1-\lambda V\tilde{\chi}_{\rm H})^{-1} = \tilde{\chi}_{\rm H} + \lambda\tilde{\chi}_{\rm H}V\tilde{\chi}_{\rm H}(1-\lambda V\tilde{\chi}_{\rm H})^{-1}, \quad (2)$$

where $\tilde{\chi}_{\rm H}$ is the single-particle density response function calculated from the SCH bands [45], summing over independent contributions from all four flavors:

$$\tilde{\chi}_{\rm H} = \sum_{f=1}^{4}\tilde{\chi}_{\rm H}^{f}. \quad (3)$$

Possible improvements to this approximation are discussed later.

When inserted in Eq. (1), the second form for the right-hand-side of Eq. (2) separates the exchange energy $E_{\rm x}$, the contribution that is first order in V, from the full fluctuation correction $E_{\rm xc} \equiv E_{\rm x} + E_{\rm c}$, allowing us to carefully account for its subtly convergent frequency integral. After integrating over λ, the exchange energy can be rewritten in the standard Slater determinant form [44]

$$E_{\rm x} = -\frac{1}{2A}{\sum_{\mathbf{q},\mathbf{g}}}' V_{\mathbf{q}+\mathbf{g}} \sum_{\substack{f,\mathbf{k},\alpha\beta,\\ \mathbf{g}_1,\mathbf{g}_2}} \delta\rho^{f}_{\alpha,\mathbf{g}_1+\mathbf{g};\beta,\mathbf{g}_2+\mathbf{g}}(\mathbf{k}+\mathbf{q}) \times [\delta\bar{\rho}^{f}(\mathbf{k}) + 2\bar{\rho}^{0f}(\mathbf{k})]_{\alpha,\mathbf{g}_1;\beta,\mathbf{g}_2}, \quad (4)$$

where $\delta\rho^{f}(\mathbf{k}) = \sum_n(\hat{z}_n(\mathbf{k})\hat{z}_n^{\dagger}(\mathbf{k})\Theta_{n\mathbf{k}} - \hat{z}^0_n(\mathbf{k})\hat{z}^{0\dagger}_n(\mathbf{k})\Theta^0_{n\mathbf{k}})$ is the density matrix projected to flavor f relative to that of a charge neutral decoupled bilayer, $\delta\bar{\rho}$ is the complex conjugate of the corresponding matrix element of $\delta\rho$, $\hat{z}_n(\mathbf{k})$ and $\hat{z}^0_n(\mathbf{k})$ are plane-wave representation SCH and neutral-decoupled-bilayer quasiparticle eigenvectors, and $\Theta_{n\mathbf{k}}$ and $\Theta^0_{n\mathbf{k}}$ are the corresponding occupation numbers. In Eq. (4) $\mathbf{g}, \mathbf{g}_1, \mathbf{g}_2$ are moiré reciprocal lattice vectors, $\mathbf{k}$ and $\mathbf{q}$ are momenta in MBZ, α and β are layer and sublattice indices and A is the area of the 2D system. Because of their negative energy seas, continuum models of graphene multilayers are able to determine total energies only up to a reference energy (per area) that is a linear functions of electron density, $\varepsilon_{\rm ref} = \varepsilon_0 + \mu_0 n$; Eq. (4) chooses the zero of energy ε_0 to be the energy per area of neutral decoupled bilayers and the zero of chemical potential μ_0 to be the energy of states at the top of the decoupled bilayer valence band. The integration over the coupling constant λ in Eq. (1) can be performed analytically to yield the correlation energy [44]

$$E_{\rm c} = \frac{1}{2\pi}{\sum_{\mathbf{q}}}' \int_0^{\infty} d\omega {\rm Tr}\left[\sqrt{\mathbf{V}}\tilde{\boldsymbol{\chi}}_{\rm H}\sqrt{\mathbf{V}} + \ln(1-\sqrt{\mathbf{V}}\tilde{\boldsymbol{\chi}}_{\rm H}\sqrt{\mathbf{V}})\right], \quad (5)$$

where $\mathbf{V}$ and $\tilde{\boldsymbol{\chi}}_{\rm H}$ are matrices in reciprocal lattice vector with implicit $\mathbf{q}$ and ω dependences. The correlation energy must be regularized by subtracting its value in unbroken symmetry states at CN; its contribution to the chemical potential at CN is close to zero because the models we study have approximate particle-hole symmetry.

Paramagnetic State Energy. We interpret our numerical results for the band filling ν dependence of the MATBG paramagnetic ground-state energy [Figs. 2(b) and 2(c)] by comparing them with results for the decoupled bilayer [46] [Fig. 2(a)] calculated in exactly the same way. In both cases the exchange energy is positive at small $|\nu|$ because of [46] rapid changes in Bloch state spinors near the Dirac point. The blue dashed line in Fig. 2(a) is the exchange energy of an eight-Dirac-cone model [46]

$$E_{\rm x}^{\rm D} = \frac{\alpha\hbar c}{24\pi}\frac{g}{\epsilon_{\rm BN}}k_{\rm F}^3 \ln\left(\frac{k_{\rm c}}{k_{\rm F}}\right) + \text{regular terms}, \quad (6)$$

where $g = 8$ and $k_{\rm F} = (4\pi n/g)^{1/2}$. The exchange energy of MATBG is smaller than that of the decoupled bilayers because of the dominant role of the Hartree potential in shaping teh occupied band states' wave functions. In contrast to the decoupled bilayer case, MATBG correlation energies are low near CN because that is where the phase space for low-energy particle-hole excitations within the flat band octet is the largest. The correlation energy is highest near $|\nu| = 4$ because the gaps between flat and remote bands suppress fluctuations. In our calculations there is a small particle-hole asymmetry in all properties, including the exchange and correlation energies, because we include nonlocal interlayer tunneling corrections [47] to the Bistritzer-MacDonald (BM) MATBG model [1,44].

Because of the partial cancellation between exchange and correlation effects, discussed again below in connection with flavor ferromagnetism, the difference between MATBG and the decoupled bilayers is dominated by the SCH energy [44] plotted in Fig. 2(c). The SCH energy is calculated relative to its value at CN, and its slope at CN is finite because the bare flat bands are centered around $\varepsilon_{\rm fb} \approx 12$ meV (see Fig. 1) in the nonlocal BM model we employ. The chemical potential μ, the energy to add a single-electron increases steadily as the flat bands are filled mainly because of Hartree effects. We find that the chemical potential difference between full and empty flat bands is ∼50 meV. When the bands are nearly empty, added electrons occupy regions in the moiré unit cell in which the mean-field potential from remote band electrons is most attractive. When the bands are nearly filled, however, it follows from approximate particle-hole symmetry that electrons occupy the same region but the Hartree mean-field potential is now repulsive.

In Fig. 2(d) we compare our results for the filling factor dependence of the chemical potential across the full range of flat band filling with experimental results published in Ref. [19]. The total shift in chemical potential is somewhat larger in the experiment than in the theory. Since the states near the full and empty flat band limit are not expected to be strongly correlated, we attribute this small discrepancy to weak mixing between flat and remote bands and small inaccuracies in the continuum model we employ. The most striking feature of these results is shared between the theory and experiment, namely, that the chemical potential increases approximately linearly with band filling factor [19,20,48,49]. In MATBG experiments, structures do emerge at some filling factors that are thought to be due to first-order flavor-symmetry breaking phase transitions at low temperatures, which we now

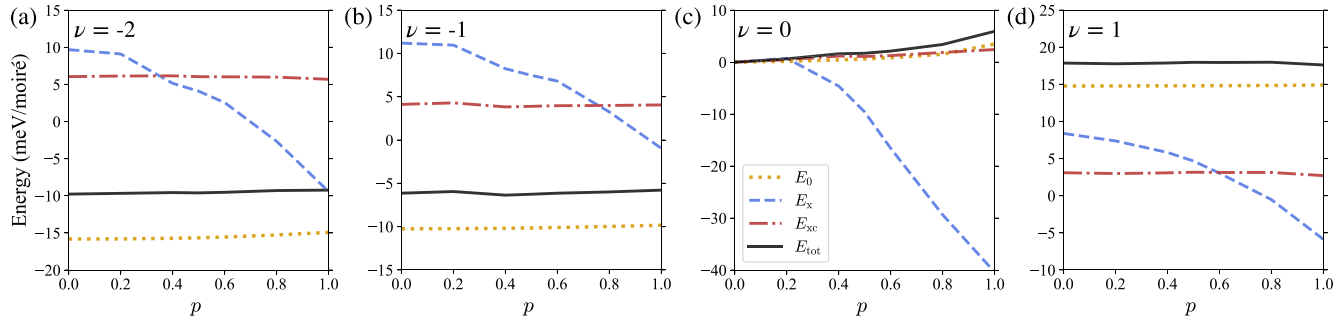

FIG. 3. SCH energy E_0 (yellow dotted lines), exchange energy E_x (blue dashed lines), exchange-correlation energy E_{xc} (red dash-dotted lines), and RPA total energy E_{tot} (black solid lines) as a function of polarization p at (a) $\nu = -2$, (b) $\nu = -1$, (c) $\nu = 0$, and (d) $\nu = 1$. p characterizes the degree of flavor polarization as explained in the main text. $p = 0$ corresponds to the paramagnetic state and $p = 1$ corresponds to full flavor polarization.

address, and at higher temperatures to surviving local moment fluctuations [50].

Flat Band Flavor Ferromagnetism. The RPA energy calculation can be carried out for any set of flavor-dependent filling factors. Typical numerical results [51] are summarized in Fig. 3. The $\nu = 0$ polarized states in Fig. 3(c) have filling factor p for two flavors and filling factor $-p$ for the other two flavors. Increasing p shifts states from the valence bands of two flavors to the conduction bands of the other two flavors. Because of MATBG's approximate particle-hole symmetry, this polarization path does not strongly influence the charge density, which remains approximately uniform at this filling factor for all values of p, as illustrated in Figs. S10 and S11. The main point to notice is that fully polarized states are strongly favored by exchange energies, but this energy gain is almost perfectly canceled by the correlation energy which strongly favors states in which each flavor is half filled. Similar results are obtained at other filling factors. The family of polarized states at $\nu = -2$ in Fig. 3(a) have filling factor $-(1 + p)/2$ for two flavors and filling factor $-(1 - p)/2$ for the other two flavors; increasing p shifts electrons between valence bands with different flavors and the charge density is nonuniform at all values of p. For $\nu = \pm 1$, the flavor polarization path illustrated in Figs. 3(b) and 3(d) is $\nu = \pm(1 + 3p)/4$ for one flavor and $\nu = \pm(1 - p)/4$ for the remaining three flavors. The exchange energy gain upon polarization is again almost exactly canceled by correlation, underscoring the dominance of the SCH energy. Once correlations are included the dependence of the SCH energy on p, which was judged to be insignificant in previous self-consistent Hartree-Fock [52] calculations, retains a role in the energy competition among different polarized states.

Within the RPA theory the cancellation between exchange and correlation for the polarization p dependence of the energy can be understood in terms of Eqs. (1) and (2). The p dependence of energy follows from that of $\tilde{\chi}_H$, and this lies mainly in the range of low-frequency fluctuations within the flat band where the important matrix elements of $V\tilde{\chi}_H$ are much larger than 1 so that $\chi(\lambda) \to V^{-1}$ (perfect screening), and the dependence of E_{xc} on polarization is lost. Physically, correlations are already strong even in the paramagnetic state and there is little left to gain by flavor ordering. Generally speaking, we find that the tendency toward flavor symmetry breaking is stronger at larger $|\nu|$ and stronger at positive ν than at negative ν, as summarized in Fig. S7, in agreement with most experiments [16,19,48,53]. In addition we find that the difference in energy between polarized and paramagnetic states is drastically reduced by correlations from ∼40 meV per moiré period to less than ∼3 meV [Fig. 3(c)].

In MATBG broken C_2T symmetry opens up a gap between the conduction and valence bands. This type of broken symmetry within flavors is therefore common in mean-field calculations. In our RPA calculations we find, as summarized in Table S2, that when C_2T symmetry is broken by adding a sublattice-dependent potential of the type produced by aligned hBN substrates, flavor ferromagnetism is favored at almost all filling factors including those proximate to CN. This finding aligns well with experimental evidence suggesting that hBN alignment tends to favor states with broken symmetries [14,15,54], including quantum anomalous Hall states at fractional flat band fillings [14].

Magic-Angle Correlation Problem. In this Letter we report on the first RPA calculation for MATBG. The RPA weak-coupling approach has the advantage that it accounts for dynamic screening of long-range Coulomb interactions, but is less reliable than some other methods in accounting for short-distance correlations. Competing methods often require tight-binding models, which in the case of MATBG have the disadvantage that they require the introduction of additional bands [55] to compensate for fragile topology inherited from the isolated layer Dirac cones. Our theory establishes the crucial influence of correlations in compressible metallic states in expanding unbroken symmetry regions in the MATBG phase diagram. The RPA weak-coupling approach is also relevant for other moiré materials that exhibit strong correlations.

Our calculations include 146 remote valence and conduction bands per spin and flavor. Our calculations are consistent with experimental indications that flavor ferromagnetism is common in both insulating and metallic states when the MATBG flat bands are partially filled, less likely close to CN, and more likely at positive filling factors than at negative filling factors. The exchange energy gains that favor broken symmetry insulating ground states at integer ν, are comparable in size to correlation energy gains in closely competing metallic states with fewer or no broken symmetries. The resulting weak dependence of energy on the magnetic state is consistent with small collective excitation energies of insulating states [56,57] and with strong coupling

approaches [22,58] that can be applied close to integer band fillings. Our calculations demonstrate that [44] fluctuations in remote bands do not generally play a central role in MATBG properties except in the cases of nearly empty and nearly full bands. This finding justifies the flat-band projection that is required to make nonperturbative finite-size numerical calculations [59–62] feasible. Perturbative calculations are approximate, but have the advantage that finite-size effects can be eliminated by taking dense momentum space grids; our calculations employ 432 k-points in the MBZ.

Our calculations can be compared directly to experimental results for the chemical potential μ, which increases by $\sim$50 meV as the flat bands are filled. This compares to a dependence of energy on flavor polarization that is typically $\sim$3 meV per moiré cell. The positive compressibility we find, in agreement with the experiment, for MATBG electrons contrasts with the well-known negative compressibility of strongly interacting two-dimensional electron gas systems [63,64], and is associated with unusual properties of the projected flat-band Hilbert space. In MATBG models with exact particle-hole symmetry, the flat conduction and valence bands at the Fermi energy spatial structure within the moiré unit cell that precisely complements the total density of remote occupied bands, so that the total density is uniform. The increase in chemical potential with filling factor is associated with the property that the nonuniform density of the remote bands is first eliminated and then restored with the opposite sign as the flat bands are filled. We emphasize that, unlike most calculations in the literature, which overstate dielectric screening to suppress interaction scales, all our results are obtained using a physically realistic hBN dielectric constant ϵ_{BN}=5.1 [44].

The MATBG correlation problem is extraordinarily challenging and the RPA theory, like other approaches, has limitations. Even though the flat band eigenstates have weak dispersion, their wave functions vary in a complex way across the MBZ. For this reason there is no simple Hubbard-like lattice model representation of the correlation problem. Aside from the fascinating low-temperature superconducting instability, two key higher-energy issues still do not have definitive answers. (i) What is the ground state at CN? Is it the $p=0$ state of Fig. 3, which has no broken symmetries and strong correlations, or the $p=1$ state, which is a single Slater determinant with analytically calculable excitations when remote band fluctuations are neglected? (ii) What is the Fermi surface in the range of filling factors surrounding $\nu=0$? Is it the γ centered Fermi surface of the $p=1$ state or the κ,κ' centered Fermi surface of the $p=0$ state? In either case how does the Fermi surface, at least as indicated by weak-field Hall measurements [47], manage to avoid Lifshitz transitions over such a broad range of filling factors $-1.8 \lesssim \nu \lesssim 0.9$ surrounding $\nu=0$? For the first question we do not consider the weak-coupling answer (that $p=0$ is favored) to be definitive, but it certainly demonstrates that the two states are competitive. The second question is especially troublesome if one imagines that the ground state near $\nu=0$ is a doped $p=1$ state in which the band degeneracies have been reduced from four to two and the Fermi surface areas must be correspondingly larger. The more likely option, in our view, is that the ground state near CN is an unpolarized state as predicted by RPA. Part of the motivation for this view is the absence of finite-temperature anomalies in the experiment, which would signal a phase transitions to a paramagnetic state — expected to be at least weakly first order in MATBG as in other itinerant electron magnets [65]. If so, there is no hint experimentally of the emergence between $\nu=0$ and $|\nu|=1$ of the self-consistent Hartree multipocket Fermi surface topology illustrated in Fig. 1. Future work should explain why this pocket does not appear (or alternately why its appearance does not influence transport), perhaps due to a refinement of the single-particle model which changes flat band wave functions [66–69], exchange interactions within the doped flat bands that stabilize κ,κ' centered surfaces, broken C_2T symmetry related to chiral model physics [22,56,70,71], and intervalley exchange interactions that we neglected [71–73]. Systematic studies of the evolution of MATBG properties with gate-induced interlayer displacement fields could play a role in sorting this confusing landscape.

Acknowledgments. Work in Austin was supported by the U.S. Department of Energy, Office of Science, Basic Energy Sciences, under Award No. DE-SC0019481. M.P. is supported by the European Union's Horizon 2020 research and innovation program under the Grant Agreement No. 881603 - GrapheneCore3 and the Marie Sklodowska-Curie Grant Agreement No. 873028 and by the MUR - Italian Minister of University and Research under the "Research projects of relevant national interest - PRIN 2020" - Project No. 2020JLZ52N, title "Light-matter interactions and the collective behavior of quantum 2D materials (q-LIMA)". The authors acknowledge resources provided by the Texas Advanced Computing Center (TACC) at The University of Texas at Austin that have contributed to the research results reported in this paper.

[1] R. Bistritzer and A. H. MacDonald, Moiré bands in twisted double-layer graphene, Proc. Natl. Acad. Sci. **108**, 12233 (2011).

[2] Y. Cao, V. Fatemi, S. Fang, K. Watanabe, T. Taniguchi, E. Kaxiras, and P. Jarillo-Herrero, Unconventional superconductivity in magic-angle graphene superlattices, Nature (London) **556**, 43 (2018).

[3] Y. Cao, V. Fatemi, A. Demir, S. Fang, S. L. Tomarken, J. Y. Luo, J. D. Sanchez-Yamagishi, K. Watanabe, T. Taniguchi, E. Kaxiras, R. C. Ashoori, and P. Jarillo-Herrero, Correlated insulator behaviour at half-filling in magic-angle graphene superlattices, Nature (London) **556**, 80 (2018).

[4] E. Y. Andrei and A. H. MacDonald, Graphene bilayers with a twist, Nat. Mater. **19**, 1265 (2020).

[5] L. Balents, C. R. Dean, D. K. Efetov, and A. F. Young, Superconductivity and strong correlations in moiré flat bands, Nat. Phys. **16**, 725 (2020).

[6] E. McCann and V. I. Fal'ko, Landau-level degeneracy and quantum Hall effect in a graphite bilayer, Phys. Rev. Lett. **96**, 086805 (2006).
[7] Y. Barlas, R. Côté, K. Nomura, and A. H. MacDonald, Intra-landau-level cyclotron resonance in bilayer graphene, Phys. Rev. Lett. **101**, 097601 (2008).
[8] R. Côté, J. Lambert, Y. Barlas, and A. H. MacDonald, Orbital order in bilayer graphene at filling factor $\nu = -1$, Phys. Rev. B **82**, 035445 (2010).
[9] Y. Barlas, K. Yang, and A. H. MacDonald, Quantum Hall effects in graphene-based two-dimensional electron systems, Nanotechnology **23**, 052001 (2012).
[10] B. E. Feldman, J. Martin, and A. Yacoby, Broken-symmetry states and divergent resistance in suspended bilayer graphene, Nat. Phys. **5**, 889 (2009).
[11] J. Martin, B. E. Feldman, R. T. Weitz, M. T. Allen, and A. Yacoby, Local compressibility measurements of correlated states in suspended bilayer graphene, Phys. Rev. Lett. **105**, 256806 (2010).
[12] R. T. Weitz, M. T. Allen, B. E. Feldman, J. Martin, and A. Yacoby, Broken-symmetry states in doubly gated suspended bilayer graphene, Science **330**, 812 (2010).
[13] J. Jung, F. Zhang, and A. H. MacDonald, Lattice theory of pseudospin ferromagnetism in bilayer graphene: Competing interaction-induced quantum Hall states, Phys. Rev. B **83**, 115408 (2011).
[14] M. Serlin, C. L. Tschirhart, H. Polshyn, Y. Zhang, J. Zhu, K. Watanabe, T. Taniguchi, L. Balents, and A. F. Young, Intrinsic quantized anomalous Hall effect in a moiré heterostructure, Science **367**, 900 (2020).
[15] A. L. Sharpe, E. J. Fox, A. W. Barnard, J. Finney, K. Watanabe, T. Taniguchi, M. A. Kastner, and D. Goldhaber-Gordon, Emergent ferromagnetism near three-quarters filling in twisted bilayer graphene, Science **365**, 605 (2019).
[16] P. Stepanov, M. Xie, T. Taniguchi, K. Watanabe, X. Lu, A. H. MacDonald, B. A. Bernevig, and D. K. Efetov, Competing zero-field Chern insulators in superconducting twisted bilayer graphene, Phys. Rev. Lett. **127**, 197701 (2021).
[17] X. Lu, P. Stepanov, W. Yang, M. Xie, M. A. Aamir, I. Das, C. Urgell, K. Watanabe, T. Taniguchi, G. Zhang, A. Bachtold, A. H. MacDonald, and D. K. Efetov, Superconductors, orbital magnets and correlated states in magic-angle bilayer graphene, Nature (London) **574**, 653 (2019).
[18] H. Polshyn, J. Zhu, M. A. Kumar, Y. Zhang, F. Yang, C. L. Tschirhart, M. Serlin, K. Watanabe, T. Taniguchi, A. H. MacDonald, and A. F. Young, Electrical switching of magnetic order in an orbital Chern insulator, Nature (London) **588**, 66 (2020).
[19] U. Zondiner, A. Rozen, D. Rodan-Legrain, Y. Cao, R. Queiroz, T. Taniguchi, K. Watanabe, Y. Oreg, F. von Oppen, A. Stern, E. Berg, P. Jarillo-Herrero, and S. Ilani, Cascade of phase transitions and dirac revivals in magic-angle graphene, Nature (London) **582**, 203 (2020).
[20] D. Wong, K. P. Nuckolls, M. Oh, B. Lian, Y. Xie, S. Jeon, K. Watanabe, T. Taniguchi, B. A. Bernevig, and A. Yazdani, Cascade of electronic transitions in magic-angle twisted bilayer graphene, Nature (London) **582**, 198 (2020).
[21] I. Das, X. Lu, J. Herzog-Arbeitman, Z.-D. Song, K. Watanabe, T. Taniguchi, B. A. Bernevig, and D. K. Efetov, Symmetry-broken Chern insulators and rashba-like landau-level crossings in magic-angle bilayer graphene, Nat. Phys. **17**, 710 (2021).
[22] E. Khalaf, S. Chatterjee, N. Bultinck, M. P. Zaletel, and A. Vishwanath, Charged skyrmions and topological origin of superconductivity in magic-angle graphene, Sci. Adv. **7**, eabf5299 (2021).
[23] Y. Saito, F. Yang, J. Ge, X. Liu, T. Taniguchi, K. Watanabe, J. I. A. Li, E. Berg, and A. F. Young, Isospin pomeranchuk effect in twisted bilayer graphene, Nature (London) **592**, 220 (2021).
[24] Y. Xie, A. T. Pierce, J. M. Park, D. E. Parker, E. Khalaf, P. Ledwith, Y. Cao, S. H. Lee, S. Chen, P. R. Forrester, K. Watanabe, T. Taniguchi, A. Vishwanath, P. Jarillo-Herrero, and A. Yacoby, Fractional Chern insulators in magic-angle twisted bilayer graphene, Nature (London) **600**, 439 (2021).
[25] S. Wu, Z. Zhang, K. Watanabe, T. Taniguchi, and E. Y. Andrei, Chern insulators, van Hove singularities and topological flat bands in magic-angle twisted bilayer graphene, Nat. Mater. **20**, 488 (2021).
[26] K. P. Nuckolls, M. Oh, D. Wong, B. Lian, K. Watanabe, T. Taniguchi, B. A. Bernevig, and A. Yazdani, Strongly correlated Chern insulators in magic-angle twisted bilayer graphene, Nature (London) **588**, 610 (2020).
[27] J. Kang and O. Vafek, Strong coupling phases of partially filled twisted bilayer graphene narrow bands, Phys. Rev. Lett. **122**, 246401 (2019).
[28] B. Lian, Z.-D. Song, N. Regnault, D. K. Efetov, A. Yazdani, and B. A. Bernevig, Twisted bilayer graphene. IV. exact insulator ground states and phase diagram, Phys. Rev. B **103**, 205414 (2021).
[29] X. Liu, G. Farahi, C.-L. Chiu, Z. Papic, K. Watanabe, T. Taniguchi, M. P. Zaletel, and A. Yazdani, Visualizing broken symmetry and topological defects in a quantum Hall ferromagnet, Science **375**, 321 (2022).
[30] L. Wang, E.-M. Shih, A. Ghiotto, L. Xian, D. A. Rhodes, C. Tan, M. Claassen, D. M. Kennes, Y. Bai, B. Kim, K. Watanabe, T. Taniguchi, X. Zhu, J. Hone, A. Rubio, A. N. Pasupathy, and C. R. Dean, Correlated electronic phases in twisted bilayer transition metal dichalcogenides, Nat. Mater. **19**, 861 (2020).
[31] T. Wang, D. E. Parker, T. Soejima, J. Hauschild, S. Anand, N. Bultinck, and M. P. Zaletel, Ground-state order in magic-angle graphene at filling $\nu = -3$: A full-scale density matrix renormalization group study, Phys. Rev. B **108**, 235128 (2023).
[32] J. Zhu, J.-J. Su, and A. H. MacDonald, Voltage-controlled magnetic reversal in orbital Chern insulators, Phys. Rev. Lett. **125**, 227702 (2020).
[33] These statements are based on a minimal interpretation of measurements of electronic compressibility [19], tunneling spectroscopy [20], and weak-field Hall effects [47]. Other scenarios in which flavor symmetries are broken even at CN cannot be ruled out at present and are assumed in some theoretical work. Note that the cascades observed in the high-temperature compressibility experiment [23] (up to 100 K) are not indicative of ground-state phase transitions. These high-temperature cascades may result from fluctuations of local moments, which can be explained by localized orbitals and the heavy fermion model [58,74].
[34] D. Golze, M. Dvorak, and P. Rinke, The GW compendium: A practical guide to theoretical photoemission spectroscopy, Frontiers in Chemistry **7**, 377 (2019).

[35] J. Deslippe, G. Samsonidze, D. A. Strubbe, M. Jain, M. L. Cohen, and S. G. Louie, Berkeleygw: A massively parallel computer package for the calculation of the quasiparticle and optical properties of materials and nanostructures, Comput. Phys. Commun. **183**, 1269 (2012).

[36] M. Gell-Mann and K. A. Brueckner, Correlation energy of an electron gas at high density, Phys. Rev. **106**, 364 (1957).

[37] T. Olsen and K. S. Thygesen, Random phase approximation applied to solids, molecules, and graphene-metal interfaces: From Van der Waals to covalent bonding, Phys. Rev. B **87**, 075111 (2013).

[38] T. Olsen, Assessing the performance of the random phase approximation for exchange and superexchange coupling constants in magnetic crystalline solids, Phys. Rev. B **96**, 125143 (2017).

[39] M. Xie and A. H. MacDonald, Nature of the correlated insulator states in twisted bilayer graphene, Phys. Rev. Lett. **124**, 097601 (2020).

[40] F. Guinea and N. R. Walet, Electrostatic effects, band distortions, and superconductivity in twisted graphene bilayers, Proc. Natl. Acad. Sci. **115**, 13174 (2018).

[41] T. Cea, N. R. Walet, and F. Guinea, Electronic band structure and pinning of fermi energy to van Hove singularities in twisted bilayer graphene: A self-consistent approach, Phys. Rev. B **100**, 205113 (2019).

[42] L. Rademaker, D. A. Abanin, and P. Mellado, Charge smoothening and band flattening due to Hartree corrections in twisted bilayer graphene, Phys. Rev. B **100**, 205114 (2019).

[43] T. Cea and F. Guinea, Band structure and insulating states driven by coulomb interaction in twisted bilayer graphene, Phys. Rev. B **102**, 045107 (2020).

[44] See Supplemental Material at http://link.aps.org/supplemental/10.1103/PhysRevB.110.L121117 for the derivation of Eq. (1) in SM II; the derivations of Eqs. (4) and (5) in SM VII; the definition of SCH energy E_0 in SM III; the expression of $\rho^{0f}(\mathbf{k})$ in Eq. (4) in SM VIII; details of MATBG model parameters that we use in this article in SM I; a detailed discussion on fluctuations in remote bands in SM IX; Fig. S12 for the energy dependence on dielectric constant ϵ_{BN}; and which includes Refs. [1,22,47,66–69,75–85].

[45] P. Novelli, I. Torre, F. H. L. Koppens, F. Taddei, and M. Polini, Optical and plasmonic properties of twisted bilayer graphene: Impact of interlayer tunneling asymmetry and ground-state charge inhomogeneity, Phys. Rev. B **102**, 125403 (2020).

[46] Y. Barlas, T. Pereg-Barnea, M. Polini, R. Asgari, and A. H. MacDonald, Chirality and correlations in graphene, Phys. Rev. Lett. **98**, 236601 (2007).

[47] M. Xie and A. H. MacDonald, Weak-field Hall resistivity and spin-valley flavor symmetry breaking in magic-angle twisted bilayer graphene, Phys. Rev. Lett. **127**, 196401 (2021).

[48] S. L. Tomarken, Y. Cao, A. Demir, K. Watanabe, T. Taniguchi, P. Jarillo-Herrero, and R. C. Ashoori, Electronic compressibility of magic-angle graphene superlattices, Phys. Rev. Lett. **123**, 046601 (2019).

[49] T. Cea, P. A. Pantaleón, N. R. Walet, and F. Guinea, Electrostatic interactions in twisted bilayer graphene, Nano Materials Science **4**, 27 (2022).

[50] One important limitation of the weak-coupling approach is that it does not capture the influence of unordered fluctuating local moments.

[51] A more complete set of numerical results for a wide variety of filling factors and flavor polarizations are gathered in SM X Table S1.

[52] S. Liu, E. Khalaf, J. Y. Lee, and A. Vishwanath, Nematic topological semimetal and insulator in magic-angle bilayer graphene at charge neutrality, Phys. Rev. Res. **3**, 013033 (2021).

[53] M. Yankowitz, S. Chen, H. Polshyn, Y. Zhang, K. Watanabe, T. Taniguchi, D. Graf, A. F. Young, and C. R. Dean, Tuning superconductivity in twisted bilayer graphene, Science **363**, 1059 (2019).

[54] A. L. Sharpe, E. J. Fox, A. W. Barnard, J. Finney, K. Watanabe, T. Taniguchi, M. A. Kastner, and D. Goldhaber-Gordon, Evidence of orbital ferromagnetism in twisted bilayer graphene aligned to hexagonal boron nitride, Nano Lett. **21**, 4299 (2021).

[55] H. C. Po, L. Zou, T. Senthil, and A. Vishwanath, Faithful tight-binding models and fragile topology of magic-angle bilayer graphene, Phys. Rev. B **99**, 195455 (2019).

[56] E. Khalaf, N. Bultinck, A. Vishwanath, and M. P. Zaletel, Soft modes in magic angle twisted bilayer graphene, arXiv:2009.14827.

[57] A. Kumar, M. Xie, and A. H. MacDonald, Lattice collective modes from a continuum model of magic-angle twisted bilayer graphene, Phys. Rev. B **104**, 035119 (2021).

[58] Z.-D. Song and B. A. Bernevig, Magic-angle twisted bilayer graphene as a topological heavy fermion problem, Phys. Rev. Lett. **129**, 047601 (2022).

[59] P. Potasz, M. Xie, and A. H. MacDonald, Exact diagonalization for magic-angle twisted bilayer graphene, Phys. Rev. Lett. **127**, 147203 (2021).

[60] C. Repellin, Z. Dong, Y.-H. Zhang, and T. Senthil, Ferromagnetism in narrow bands of moiré superlattices, Phys. Rev. Lett. **124**, 187601 (2020).

[61] F. Xie, A. Cowsik, Z.-D. Song, B. Lian, B. A. Bernevig, and N. Regnault, Twisted bilayer graphene. VI. an exact diagonalization study at nonzero integer filling, Phys. Rev. B **103**, 205416 (2021).

[62] T. Soejima, D. E. Parker, N. Bultinck, J. Hauschild, and M. P. Zaletel, Efficient simulation of moiré materials using the density matrix renormalization group, Phys. Rev. B **102**, 205111 (2020).

[63] J. P. Eisenstein, L. N. Pfeiffer, and K. W. West, Negative compressibility of interacting two-dimensional electron and quasiparticle gases, Phys. Rev. Lett. **68**, 674 (1992).

[64] G. L. Yu, R. Jalil, B. Belle, A. S. Mayorov, P. Blake, F. Schedin, S. V. Morozov, L. A. Ponomarenko, F. Chiappini, S. Wiedmann, U. Zeitler, M. I. Katsnelson, A. K. Geim, K. S. Novoselov, and D. C. Elias, Interaction phenomena in graphene seen through quantum capacitance, Proc. Natl. Acad. Sci. **110**, 3282 (2013).

[65] M. Brando, D. Belitz, F. M. Grosche, and T. R. Kirkpatrick, Metallic quantum ferromagnets, Rev. Mod. Phys. **88**, 025006 (2016).

[66] S. Fang, S. Carr, Z. Zhu, D. Massatt, and E. Kaxiras, Angle-dependent ab initio low-energy Hamiltonians for a relaxed twisted bilayer graphene heterostructure, arXiv:1908.00058.

[67] S. Carr, S. Fang, Z. Zhu, and E. Kaxiras, Exact continuum model for low-energy electronic states of twisted bilayer graphene, Phys. Rev. Res. **1**, 013001 (2019).

[68] O. Vafek and J. Kang, Continuum effective Hamiltonian for graphene bilayers for an arbitrary smooth lattice deformation from microscopic theories, Phys. Rev. B **107**, 075123 (2023).

[69] J. Kang and O. Vafek, Pseudomagnetic fields, particle-hole asymmetry, and microscopic effective continuum Hamiltonians of twisted bilayer graphene, Phys. Rev. B **107**, 075408 (2023).

[70] G. Tarnopolsky, A. J. Kruchkov, and A. Vishwanath, Origin of magic angles in twisted bilayer graphene, Phys. Rev. Lett. **122**, 106405 (2019).

[71] N. Bultinck, E. Khalaf, S. Liu, S. Chatterjee, A. Vishwanath, and M. P. Zaletel, Ground state and hidden symmetry of magic-angle graphene at even integer filling, Phys. Rev. X **10**, 031034 (2020).

[72] E. Khalaf, P. Ledwith, and A. Vishwanath, Symmetry constraints on superconductivity in twisted bilayer graphene: Fractional vortices, 4*e* condensates, or nonunitary pairing, Phys. Rev. B **105**, 224508 (2022).

[73] M. Kashiwagi, T. Taen, K. Uchida, K. Watanabe, T. Taniguchi, and T. Osada, Weak localization on moiré superlattice in twisted double bilayer graphene, Jpn. J. Appl. Phys. **61**, 100907 (2022).

[74] J. Kang, B. A. Bernevig, and O. Vafek, Cascades between light and heavy fermions in the normal state of magic-angle twisted bilayer graphene, Phys. Rev. Lett. **127**, 266402 (2021).

[75] R. Geick, C. H. Perry, and G. Rupprecht, Normal modes in hexagonal boron nitride, Phys. Rev. **146**, 543 (1966).

[76] G. Giuliani and G. Vignale, *Quantum Theory of the Electron Liquid* (Cambridge University Press, Cambridge, England, 2005).

[77] A. Görling, Hierarchies of methods towards the exact kohn-sham correlation energy based on the adiabatic-connection fluctuation-dissipation theorem, Phys. Rev. B **99**, 235120 (2019).

[78] Y. H. Kwan, G. Wagner, T. Soejima, M. P. Zaletel, S. H. Simon, S. A. Parameswaran, and N. Bultinck, Kekulé spiral order at all nonzero integer fillings in twisted bilayer graphene, Phys. Rev. X **11**, 041063 (2021).

[79] P. J. Ledwith, E. Khalaf, and A. Vishwanath, Strong coupling theory of magic-angle graphene: A pedagogical introduction, Ann. Phys. (NY) **435**, 168646 (2021).

[80] G. Shavit, E. Berg, A. Stern, and Y. Oreg, Theory of correlated insulators and superconductivity in twisted bilayer graphene, Phys. Rev. Lett. **127**, 247703 (2021).

[81] G. Shavit, K. Kolář, C. Mora, F. von Oppen, and Y. Oreg, Strain disorder and gapless intervalley coherent phase in twisted bilayer graphene, Phys. Rev. B **107**, L081403 (2023).

[82] M. Oh, K. P. Nuckolls, D. Wong, R. L. Lee, X. Liu, K. Watanabe, T. Taniguchi, and A. Yazdani, Evidence for unconventional superconductivity in twisted bilayer graphene, Nature (London) **600**, 240 (2021).

[83] J. P. Hong, T. Soejima, and M. P. Zaletel, Detecting symmetry breaking in magic angle graphene using scanning tunneling microscopy, Phys. Rev. Lett. **129**, 147001 (2022).

[84] J. Yu, B. A. Foutty, Y. H. Kwan, M. E. Barber, K. Watanabe, T. Taniguchi, Z.-X. Shen, S. A. Parameswaran, and B. E. Feldman, Spin skyrmion gaps as signatures of intervalley-coherent insulators in magic-angle twisted bilayer graphene, Nat. Commun. **14**, 6679 (2023).

[85] K. P. Nuckolls, R. L. Lee, M. Oh, D. Wong, T. Soejima, J. P. Hong, D. Călugăru, J. Herzog-Arbeitman, B. A. Bernevig, K. Watanabe, T. Taniguchi, N. Regnault, M. P. Zaletel, and A. Yazdani, Quantum textures of the many-body wavefunctions in magic-angle graphene, Nature (London) **620**, 525 (2023).